Hindawi
International Journal of Corrosion
Volume 2024, Article ID 6343114, 10 pages
https://doi.org/10.1155/2024/6343114

Research Article

Corrosion Behaviour of a Cr_2O_3 Coating on Mild Steel in Synthetic Mine Water

Silas I. Hango,[1,2] **Lesley A. Cornish**,[1] **Josias W. van der Merwe**,[1] **and Lesley H. Chown**[1]

[1]*School of Chemical and Metallurgical Engineering, DSI-NRF Centre of Excellence in Strong Materials and African Materials Science and Engineering Network (AMSEN), University of the Witwatersrand, Private Bag 3, WITS, 2050 Johannesburg, South Africa*
[2]*Department of Mechanical and Metallurgical Engineering, University of Namibia, P.O. Box 3624, Ongwediva, Namibia*

Correspondence should be addressed to Silas I. Hango; shango@unam.na

Received 2 November 2023; Revised 13 March 2024; Accepted 8 April 2024; Published 22 April 2024

Academic Editor: Manikandan M

The Cr_2O_3 coating on the surface of ASTM A516 Grade 70 mild steel substrates was developed using the thermal plasma spraying process for protection against corrosion and wear. The microstructural behaviours for both coating and substrate were analysed using SEM and XRD techniques. The corrosion behaviours of the coatings and substrate in synthetic mine water with varying pH values (6, 3, and 1) were evaluated according to ASTM standards for potentiodynamic polarisation measurements. Tafel plots were drawn to determine the corrosion rates. Vickers hardness of the coatings and substrate were measured. The Cr_2O_3 coating exhibited cracks due to the solidification and cooling process, as well as some pores between the top and bonding layers caused by unmelted or partially melted particles. The corrosion tests revealed that a decrease in pH levels led to increased corrosion rates in both samples. The Cr_2O_3 coating demonstrated superior corrosion resistance, ranging from 0.036 ± 0.003 mm/year to 0.110 ± 0.004 mm/year, compared to the mild steel substrate, which ranged from 0.262 ± 0.021 mm/year to 0.336 ± 0.026 mm/year, across all pH values. Moreover, it exhibited significantly greater hardness (1260 ± 77 HV_3) than the mild steel substrate (180 ± 14 HV_3). The lower corrosion rates and higher hardness of Cr_2O_3 coating than the mild steel substrate make it a suitable coating in applications where corrosion resistance and high hardness properties are essential.

1. Introduction

ASTM A516 Grade 70 mild steel, with ~0.05–0.25 wt% C, exhibits good mechanical strength, chemical inertness, and hardness characteristics. Its availability at a relatively low cost makes it an important engineering material for construction, pump components, railway lines, automobile parts, and various industrial applications compared to carbon steels [1–5]. However, mild steel is susceptible to corrosion and wear when exposed to harsh environments, leading to surface damage and poor performance [6]. To mitigate these issues, various techniques such as thermal plasma spraying, high-velocity oxy-fuel spraying (HVOF), chemical vapour deposition, magnetron sputtering, and ion implantation have been used to provide corrosion and wear-resistant surfaces for mild steel under different operating conditions [7–9]. Plasma coating is considered the most reliable method as it produces coatings with high bond strength, thicknesses ranging from ~100 to 300 μm, and are free from oxides and porosity [3, 10, 11].

Chromium oxide serves as a coating in applications to provide corrosion protection and enhance wear resistance [12–14]. However, challenges arise from inadequate adhesion of the coating to metal substrates due to differing coefficients of thermal expansion, alongside its higher cost compared to mild steel [14–16]. Additionally, coatings often feature pores or microcracks, creating pathways for corrosive environments to reach the substrate, resulting in localised galvanic corrosion and degradation of the underlying material [4, 17, 18].

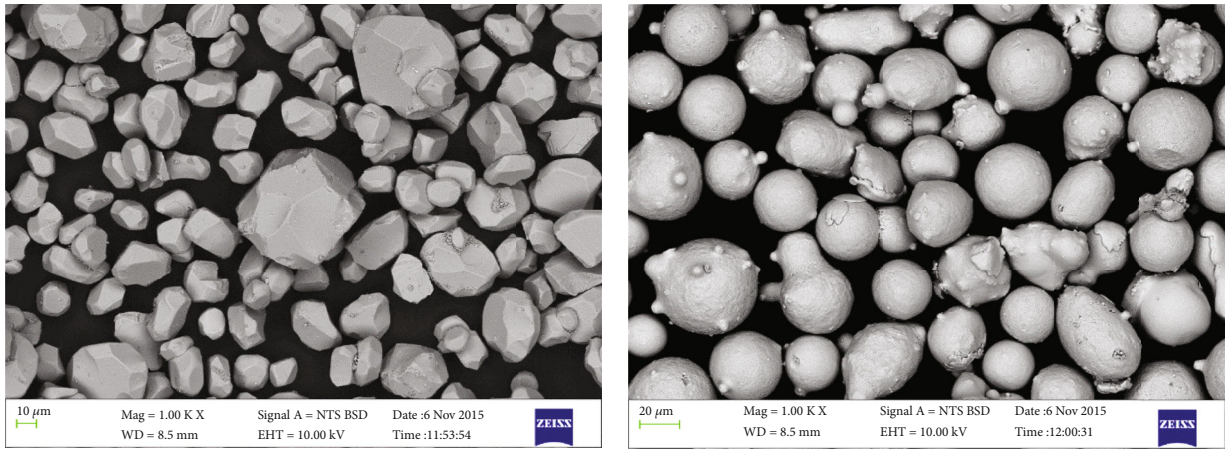

(a) (b)

Figure 1: SEM-BSE micrographs of as-received: (a) Cr_2O_3 top and (b) NiCrAlY bond coat powders [26].

Table 1: Compositions of Cr_2O_3 top, NiCrAlY bond coating powders, and mild steel substrate [26].

Sample	Element (wt%)								
	C	Cr	Ni	Fe	Si	Mn	Al	O	Y
Cr_2O_3 powder	—	Bal.	—	—		—	—	1.8 ± 0.3	
NiCrAlY powder	10.0 ± 1.0	—	Bal.	—	—		1.0 ± 0.1		1.1 ± 0.2
ASTM A516 Grade 70 mild steel	0.2 ± 0.0	—	—	Bal.	0.3 ± 0.0	1.1 ± 0.1	—	—	—

In many acidic and alkaline environments, the Cr_2O_3 coating exhibits passivation corrosion behaviour, whereby it forms a stable passive film on its surface during its interaction with the environment [19]. This passive film acts as a protective barrier, hindering the occurrence of further corrosion processes [4, 11, 20, 21].

In their research, Dong et al. [22] conducted a study on the corrosion behaviour of various Cr_2O_3-based ceramics in environments resembling supercritical water-cooled reactors. They discovered that the coatings experienced degradation due to their porous structures, leading to increased susceptibility to grain boundary attack and elevated oxygen concentrations, ultimately resulting in the dissolution of Cr_2O_3.

When Zamani et al. [23] compared the corrosion performance of Al_2O_3, Cr_2O_3, and Al_2O_3-Cr_2O_3 coatings deposited on carbon steel substrates by plasma spraying, Cr_2O_3 exhibited the best corrosion resistance in 3.5% NaCl solution.

The study by Mao et al. [24] revealed that Cr_2O_3 coating through atmospheric plasma spraying exhibited a higher hardness and wear resistance. Amanov and Berkebile [19] found that the Cr_2O_3 coating with a mean grain size of 78 nm involves the formation of nanograins, which are responsible for high hardness ranging from $1203 \pm 98\,HV_1$ to $1419 \pm 121\,HV_1$. However, Cr_2O_3 coatings are brittle and expensive [25].

This study is aimed at investigating the corrosion resistance of a Cr_2O_3 coating and a mild steel substrate when immersed in synthetic mine water, with the goal of protecting the mild steel from corrosion in the test solutions using open circuit potential and potentiodynamic polarisation measurements. Characterisation of the coating and the substrate was done using X-ray diffraction (XRD), scanning electron microscopy (SEM) with energy dispersive X-rays (EDX) techniques, and hardness measurements.

2. Materials and Methods

2.1. Materials. Commercially available Cr_2O_3 powders were used as the coating materials on ASTM A516 Grade 70 mild steel substrates. An undercoat (bond coat) of NiCrAlY powder was employed on the substrates before applying the Cr_2O_3 plasma coating. Figure 1 shows the morphologies of the as-received powders. The nominal compositions of the coating powders and the substrate are given in Table 1. The plasma spray technique was used to thermally spray the powders onto mild steel substrates.

2.2. Powder Characterisation. Before the thermal spraying process, the size and distribution of the powder particles were measured using a MS 200 Malvern Mastersizer® analyser, employing laser diffraction and water as the dispersing medium. To assess their sizes and shapes, the powders were affixed to aluminium sample holders with conductive and double-sided carbon tape for SEM-EDX analysis. X-ray diffraction (XRD) analysis was conducted on the powders using a Panalytical X'pert Pro Diffractometer equipped with Co-Kα radiation, performing scans over a range of 2θ angles from 0 to 120°, with a scan rate of 1.2° per minute and a step size of 0.02° 2θ. The Panalytical Highscore Plus analytical software was used to interpret the data.

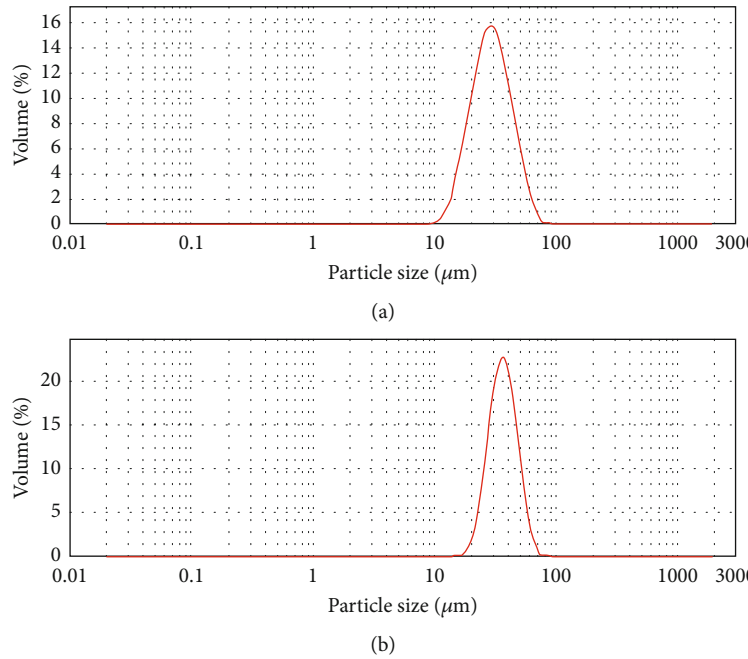

FIGURE 2: Particle size analyses of (a) Cr_2O_3 and (b) NiCrAlY powders [26].

2.3. Plasma Spray Technique. The plasma spray technique was used to apply Cr_2O_3 powders onto ASTM A516 Grade 70 mild steel substrates with a thickness of 12 mm. The substrates were cleaned ultrasonically in an alcohol bath to remove grease and dirt, then grit-blasted on one side, and the surfaces were preheated before deposition of the coatings. To enhance the adhesion between the Cr_2O_3 coatings and the mild steel substrates, NiCrAlY bond coatings were applied on mild steel substrates, followed by the application of the Cr_2O_3 top coatings. The spraying process was carried out with a SULZER METCO 9MC Plasma Control Unit, which was integrated with a FANUC System R-JS-700 robot, using parameters reported elsewhere [26]. The Cr_2O_3 powders were loaded into the plasma control feeder and then injected into a plasma jet. In this process, they were heated, melted, and injected at high velocity onto ASTM A516 Grade 70 mild steel substrates, resulting in coatings with a thickness of ~200 μm.

2.4. Microstructure and X-Ray Diffraction Characterisation. The Cr_2O_3 coatings were sectioned, hot-mounted, and wet-ground on silicon carbide papers ranging from 80 to 1200 grit. Following this, the surfaces underwent cleaning with deionised water and degreasing using acetone. The microstructures of the coating were revealed without etching, and the mild steel was etched in 3% Nital, washed under running water, rinsed in acetone to prevent overetching, and dried in an air blast. A Carl Zeiss Sigma field emission scanning electron microscope with energy dispersive X-ray spectroscopy (SEM-EDX) was used to analyse the samples. The phases were identified in the same way as for the powders (Section 2.2).

2.5. Hardness Tests. The Cr_2O_3 coating and substrate samples were prepared using metallographic techniques, following the procedures outlined in Section 2.4. Hardness tests were conducted on polished surfaces using a Vickers FM-700 hardness tester, applying a 3 kg (HV_3) load with a dwell time of 10 seconds. To ensure statistical reproducibility, the tests were performed five times, and the averages along with their standard deviations were recorded.

2.6. Corrosion Tests. The Cr_2O_3 coating and substrate samples were connected to a copper wire by aluminium conducting tape before being cold-mounted in epoxy resin for 12 hours at room temperature and then prepared as described in Section 2.4.

All corrosion tests comprising open circuit potential (OPC) and potentiodynamic polarisation [27] were conducted on the samples. These tests were carried out in synthetic mine water at pH 6 and acidified mine water at pH 3 and 1, with an exposed area of 100 mm^2. The compositions of the synthetic mine water were reported elsewhere [21]. The tests were performed using an Auto Tafel Potentiostat equipped with Auto Tafel V1.79 and Auto LPR V2.7h software. A scan rate of 0.2 mV/s was applied, scanning from -1000 mV to 600 mV versus the reference electrode potential, following a 60-minute OCP scan to ensure the values reached a steady state after the samples were immersed in the electrolyte.

Potentiodynamic polarisation measurements were carried out using a three-electrode cell configuration, with either the coated or substrate sample serving as the working electrode, a saturated calomel electrode (SCE) as the reference electrode, and graphite as the counter electrode, immersed in the electrolyte while connected to the potentiostat. These measurements started immediately when the OCPs reached their steady state after immersing the specimens in the electrolyte. A Tafel fit was employed on the potentiodynamic polarisation curves to analyse the polarisation data and calculate the corrosion current densities (i_{corr}) and corrosion rates in mm/y by

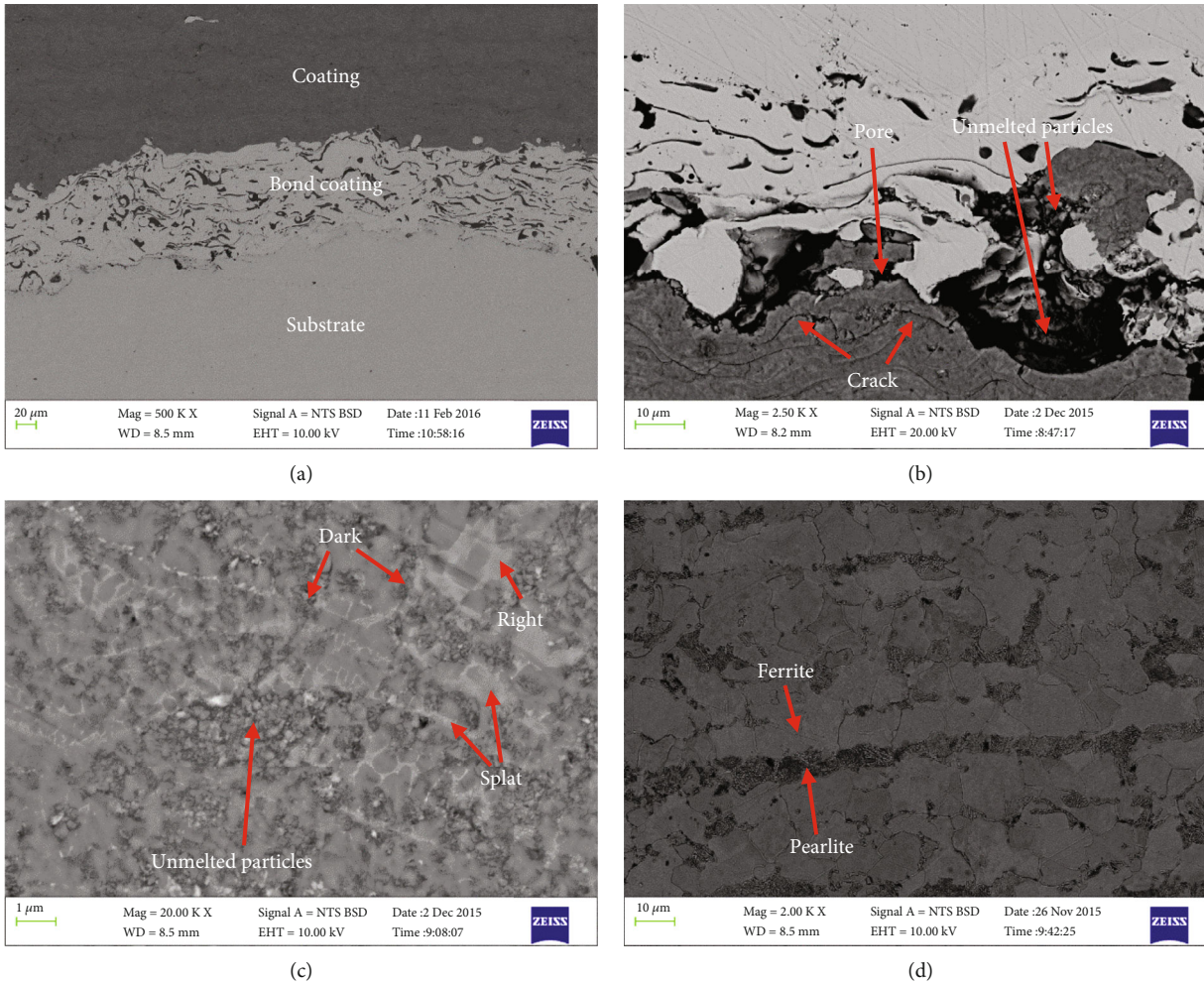

Figure 3: SEM-BSE micrographs showing the morphologies of (a) mild steel substrate-NiCrAlY bond-Cr_2O_3 top coating system; (b) NiCrAlY bond-Cr_2O_3 top coating system with pores, cracks, and unmelted particles; (c) Cr_2O_3 top coating, showing splats; and (d) mild steel substrate, showing ferrite and pearlite [26].

extrapolation of the Tafel slopes using ASTM: G102-89 standard [28]. The coatings were studied using an SEM before and after the corrosion tests.

3. Results and Discussion

3.1. Surface Morphologies and Particle Sizes of the Powders. The morphologies of the powders are given in Figure 1. The particle sizes of both the Cr_2O_3 and NiCrAlY appeared smaller in the micrographs (Figure 1) compared to the Malvern particle size analyses (Figure 2). This difference may be attributed to several factors, including the transmissivity of the carrier fluid, particle shape, angle of incidence of particles, reflectivity of particles, and carrier fluid speed [29, 30].

The Cr_2O_3 powder (Figure 1(a)) consisted of blocky, irregular, and angular particles with smooth facets, varying in size, and averaging $31.8 \pm 10.2\,\mu$m (Figure 2(a)). Conversely, the NiCrAlY powder (Figure 1(b)) comprised spherical particles, sometimes exhibiting "buds," with an average size of $38.2 \pm 1.4\,\mu$m (Figure 2(b)).

3.2. Microstructure, Energy Dispersive X-Ray Spectroscopy, and X-Ray Diffraction of the Coatings and the Substrate. Figure 3 presents the cross-sectional micrographs of the Cr_2O_3 coating on mild steel. The Cr_2O_3 coating, approximately $130\,\mu$m thick, exhibits a typical lamellar structure inherent in the plasma spray coating process and characterised by good interlayer bonding and adherence. This showed a successful coating application after the NiCrAlY bond coating (~$90\,\mu$m) had been applied to the mild steel (Figure 3(a)).

The Cr_2O_3 coating exhibited cracks (Figure 3(b)) due to residual stress during solidification [31] and cooling of the coating [32]. Additionally, there were pores observed between the top and bonding layers (Figures 3(b) and 3(c)) resulting from unmelted or partially melted particles, attributed to the difference in melting points of the powders (Cr_2O_3: 2435°C [33] and NiCrAlY: 1356°C [31], as reported by Abbasi et al. [11], Nu et al. [4], and Gerald et al. [34]. Figure 3(c) shows that the Cr_2O_3 coating displayed alternate dark and lighter splats with some unmelted particles. These unmelted particles were likely the result of insufficient heat during plasma spraying, leading to the formation of a porous layer [34]. Such characteristics are common in coatings

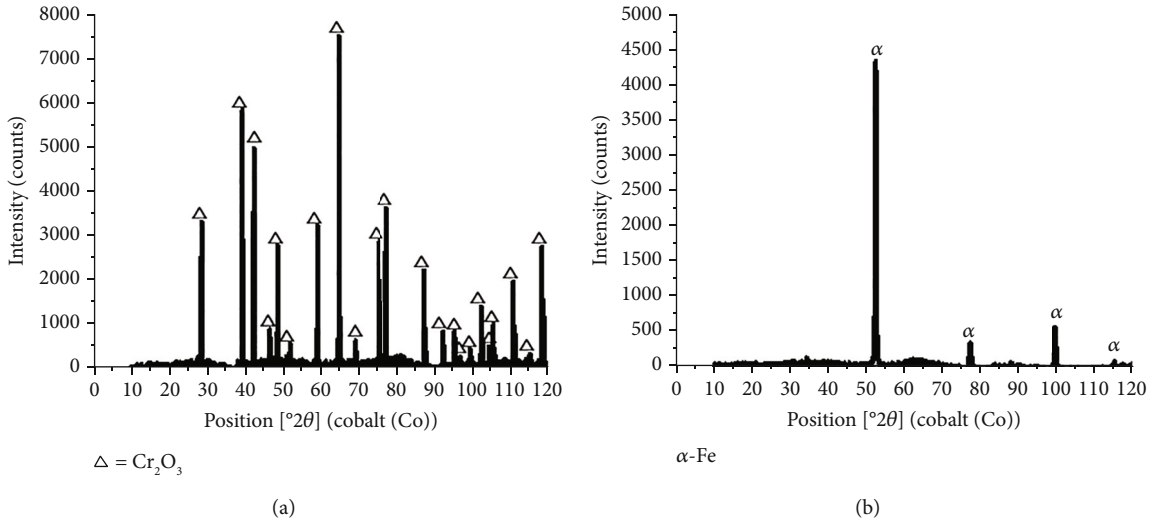

Figure 4: XRD patterns of (a) Cr_2O_3 coating and (b) mild steel substrate showing only α-ferrite.

prepared by plasma spraying, particularly in cases involving differences in melting points [4, 7, 23]. The cracks and pores present in the top coating may provide pathways for corrosive media to reach the substrate, especially considering that the bond coating also exhibited some pores [35]. In the case of mild steel (as depicted in Figure 3(d)), the microstructure revealed the presence of ferrite and pearlite, consistent with the anticipated composition and structure of mild steel.

The EDX analysis of the Cr_2O_3 coating cross-section (Figure 3(c)) revealed that the darker phase contains approximately 95.5 ± 5.4 wt% Cr and 4.5 ± 1.3 wt% O, whereas the lighter phase comprises roughly the same concentrations of chromium (95.5 ± 5.2 wt%) and oxygen (4.5 ± 1.1 wt%). In contrast, the EDX analysis for the mild steel indicated it consists predominantly of 98.5 ± 0.2 wt% Fe, with minor components of 1.2 ± 0.4 wt% Mn and less than 1 wt% Si. The XRD patterns for the Cr_2O_3 coating displayed a single-phase Cr_2O_3 structure (Figure 4(a)), which aligns with expectations from previous studies [4, 34, 36]. Meanwhile, for the mild steel substrate, only the ferrite (α) phase was identified (Figure 4(b)) [27, 37].

3.3. Hardness Measurements of the Coatings and the Substrate. As expected, Cr_2O_3 coating had a high hardness of $1260 \pm 77\ HV_3$ which agreed with values reported by Lin and Sproul [8] ($1224 \pm 153\ HV_3$) and Zamani and Valefi [15] ($1170\ HV_3$). The higher hardness of the coating can be attributed to its splat-like structure and a good interlayer bonding of single-phase composition (Figure 3(a)) [13]. The high standard deviation of Cr_2O_3 coating hardness was due to pores and unmelted particles [11], giving different local hardness values. The mild steel substrate exhibited a low hardness level of $180 \pm 14\ HV_3$ (Figure 4(b)), as expected, necessitating the application of a harder Cr_2O_3 coating for its protection.

3.4. Corrosion of the Coatings and Substrate in Synthetic Mine Water. Figure 5 shows the open circuit potentials (OCPs) for the Cr_2O_3 coating (Figure 5(a)) and mild steel (Figure 5(b)) at pH levels 6, 3, and 1, which show stabilisation over time. Initially, the OCPs trended towards more negative values during the first 1000 s, but then nearly stabilised for the remaining 3200 s. This behaviour suggests the formation of stable passive films on their surfaces or a reduction in potentials due to ion saturation in the electrolyte [38]. With a decrease in pH, the OCP for the Cr_2O_3 coating shifted towards more positive values, whereas the OCP for mild steel moved to more negative values, highlighting its greater susceptibility to corrosion compared to the Cr_2O_3 coating. These shifts demonstrate that the Cr_2O_3 coating generates more stable and effective passivating oxide films than mild steel within the test solutions [39].

Figures 5(c) and 5(d) show the potentiodynamic polarisation behaviour of Cr_2O_3 coating in synthetic mine water at varying pH values. The coating demonstrated active-passive behaviour across all pH values. The highest corrosion rate occurred at pH 1, with pH 6 experiencing the next highest rate, and pH 3 showing the lowest corrosion rate. This highest corrosion rate for the coating was mainly due to the presence of pores and cracks in the microstructure (Figure 3) [4].

The corrosion behaviour of mild steel in synthetic mine water at various pH values (Figure 5(d)) exhibited similarities, displaying active and pseudopassivation behaviour within the range of -600 mV to 600 mV, possibly attributed to the formation of pseudopassive films on the surface [26, 40]. Figures 5(c) and 5(d) indicate that chromium oxide coatings displayed superior electrochemical stability in synthetic mine water compared to mild steel, suggesting its potential as a corrosion-resistant material for mine water environments, particularly at pH 3 rather than at pH 6 and 1.

Table 2 shows the corrosion parameters recorded. The result shows that the corrosion resistance of Cr_2O_3 coatings has improved as compared to the mild steel substrate samples (0.024–0.110 mm/y vs. 0.262–0.336 mm/y). This is because the Cr_2O_3 coating has a tendency to produce a protective oxide film that acts as a barrier to the corrosive media, resulting in a low corrosion rate [3, 4, 41]. When

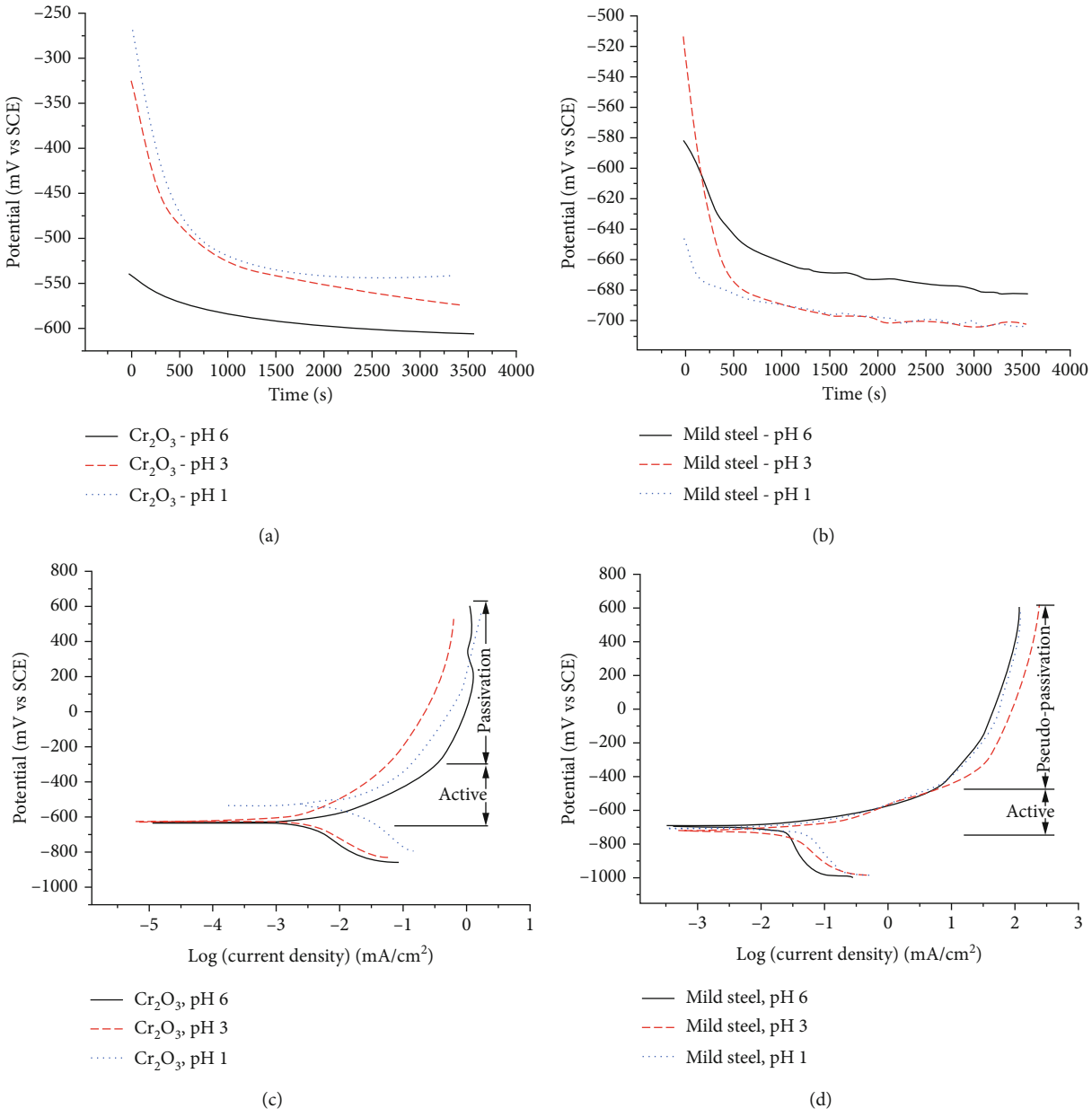

Figure 5: Open circuit potentials of (a) Cr_2O_3 coating and (b) mild steel substrate and potentiodynamic polarisation responses for (c) Cr_2O_3 coating and (d) mild steel substrate in synthetic mine water at pH 6, 3, and 1 [26].

Table 2: Potentiodynamic polarisation results of Cr_2O_3 coatings and mild steel substrates in synthetic mine water at pH 6, 3, and 1 [26].

pH	Sample	E_{corr} (mV)	i_{corr} (μA/cm^2)	Corrosion rate (mm/y)
6	Cr_2O_3 coating	−629 ± 4	2.30 ± 0.41	0.036 ± 0.003
	Mild steel	−707 ± 2	26.40 ± 2.40	0.262 ± 0.021
3	Cr_2O_3 coating	−616 ± 5	1.60 ± 0.22	0.024 ± 0.001
	Mild steel	−726 ± 1	25.00 ± 2.10	0.284 ± 0.024
1	Cr_2O_3 coating	−529 ± 4	7.20 ± 0.53	0.110 ± 0.004
	Mild steel	−724 ± 1	29.60 ± 3.10	0.336 ± 0.026

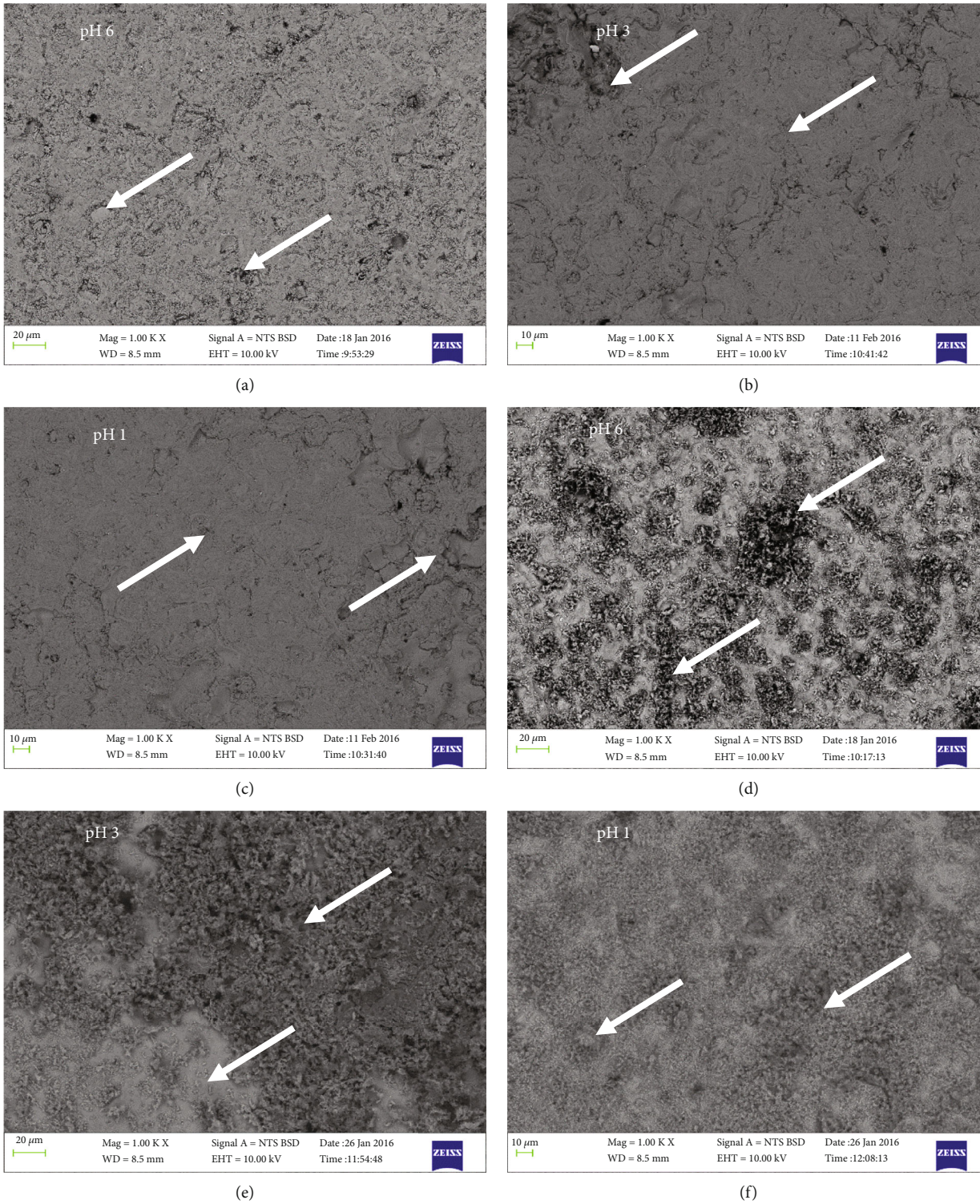

FIGURE 6: SEM-BSE micrographs of the surfaces of the (a–c) Cr_2O_3 coating and (d–f) mild steel substrate after potentiodynamic polarisation measurements in synthetic mine water at pH 6, 3, and 1, showing corrosion products (arrows) on the surfaces [26].

the pH was decreased, E_{corr} increased, and corrosion current density changed with no trend for both samples. The corrosion rates of Cr_2O_3 coating were similar to those reported by Nu et al. [4] and Abbasi et al. [11]. At pH 1, the Cr_2O_3 coating had the highest E_{corr}, i_{corr}, and corrosion rate, whereas its lowest corrosion rate was at pH 3, which was not expected. This was likely attributed to the presence of pores, cracks, and unmelted particles within the coating (Figures 3 and 6), leading to variations in corrosion behaviour in the test solutions [4, 23, 42].

Table 3: EDX analyses (in wt%) of Cr_2O_3 coating and mild steel substrate surfaces taken from Figure 6 after potentiodynamic polarisation in synthetic mine water at pH 6, 3, and 1 [26].

Sample name	Element	Composition (wt%) pH 6	pH 3	pH 1
Cr_2O_3 coating	Cr	75.0 ± 2.4	71.3 ± 4.1	73.5 ± 3.3
Mild steel substrate		—	—	—
Cr_2O_3 coating	O	23.7 ± 1.2	26.4 ± 2.3	24.8 ± 1.6
Mild steel substrate		11.3 ± 1.0	13.6 ± 3.2	14.3 ± 1.0
Cr_2O_3 coating	Na	1.3 ± 0.2	2.3 ± 0.5	1.7 ± 0.3
Mild steel substrate		2.4 ± 0.3	1.7 ± 0.0	2.1 ± 0.0
Cr_2O_3 coating	Fe	—	—	—
Mild steel substrate		83.3 ± 6.1	84.7 ± 2.0	83.6 ± 1.0

Figure 6 shows corrosion products on Cr_2O_3 coating (Figures 6(a)–6(c)) and mild steel substrate (Figures 6(d)–6(f)) surfaces after potentiodynamic polarisation in synthetic mine water. Corrosion products on the coating were notably fewer than on mild steel, suggesting lower corrosion of the coating. EDX analyses (Table 3) primarily indicated Cr and O for Cr_2O_3 and Fe and O for mild steel substrate across all pH values. The presence of Na on both surfaces, attributed to synthetic mine water composition (NaCl and Na_2SO_4), was also noted. High O EDX values suggested some O ions originated from the solution.

The primary focus of this study was to investigate the corrosion behaviour of the Cr_2O_3 coating and mild steel substrate using the potentiodynamic polarisation technique. Corrosion behaviour was further assessed through OCP, polarisation curves, XRD, and SEM with EDX. Additionally, electrochemical impedance spectroscopy (EIS) measurements will be conducted to better understand and analyse the corrosion mechanisms of the samples in the test solutions. Therefore, future research should consider incorporating EIS to enhance study findings.

4. Conclusions

The uniform distribution of Cr_2O_3 coating was successfully achieved on an ASTM A516 Grade 70 mild steel substrate using the thermal plasma spraying technique. Corrosion behaviour analysis of the Cr_2O_3 coating was evaluated through various electrochemical techniques, including OCP and potentiodynamic polarisation testing. Additionally, SEM with EDX was used for microstructural analysis, and XRD for phase identification, both before and after corrosion testing, along with hardness measurements conducted before corrosion tests. Based on the findings of this study, the following conclusions were drawn:

(1) The plasma spraying technique effectively facilitated a uniform distribution of the Cr_2O_3 coating on mild steel

(2) The hardness of the coating ($1260 \pm 77\,HV_3$) was approximately ten times greater than that of the mild steel substrate ($180 \pm 14\,HV_3$).

(3) The coating exhibited passivation behaviour, whereas the substrate displayed pseudopassivation behaviour in synthetic mine water

(4) The coating demonstrated lower corrosion rates (from 0.036 ± 0.003 mm/year to 0.110 ± 0.004 mm/year) compared to the mild steel substrate (from 0.262 ± 0.021 mm/year to 0.336 ± 0.026 mm/year) across all pH values

(5) The Cr_2O_3 coating shows promise for protecting mild steel in mining applications where high hardness and corrosion resistance are essential, owing to its superior hardness and lower corrosion rates

Data Availability

The data that support the findings of this study are available from the corresponding author upon reasonable request.

Disclosure

The manuscript was already published as a conference based on the following link: https://research.unam.edu.na/science-conference/wp-content/uploads/2022/11/ARCAENS-22-Book-of-Abstracts_final.pdf.

Conflicts of Interest

The authors declare no financial or commercial conflict of interest.

Authors' Contributions

Silas I. Hango performed the experiments, conceptualisation, investigation, and data analysis and wrote the original draft. Lesley A. Cornish, Josias W. van der Merwe, and Lesley H. Chown supervised, reviewed, and edited the work.

Acknowledgments

The authors extend their gratitude to Thermalspray (Pty) Ltd, Olifantsfontein, South Africa, for providing access to the plasma spray equipment and for supplying the Cr_2O_3 and NiCrAlY coating powders at no cost. Furthermore, the

authors would like to thank Mintek, Randburg, South Africa, for facilitating the corrosion experiments. The invaluable insights derived from the referenced doctoral thesis of the corresponding author, which served as the foundation for the findings presented in this paper, are also gratefully acknowledged. The authors would like to express their heartfelt gratitude to Frank P. L. Kavishe, who made significant contributions to this study before his passing. We honour his memory and acknowledge the profound impact he had on this research. The authors wish to acknowledge the financial support provided by the African Materials Science and Engineering Network (a Carnegie-IAS RISE Network) hosted by the University of the Witwatersrand.

References

[1] D. E. P. Klenam, L. H. Chown, M. J. Papo, and L. A. Cornish, "Steels for rail axles–an overview," *Critical Reviews in Solid State and Materials Sciences*, vol. 49, no. 2, pp. 163–193, 2024.

[2] Z. Panossian, N. L. de Almeida, R. M. de Sousa, G. de Souza Pimenta, and L. B. Marques, "Corrosion of carbon steel pipes and tanks by concentrated sulfuric acid: a review," *Corrosion Science*, vol. 58, pp. 1–11, 2012.

[3] K. S. Rao, G. C. Tejaswini, and K. G. Girisha, "Corrosion behavior of plasma sprayed Cr_2O_3–Al_2O_3–ZrO_2 multilayer coatings on mild steel," *Materials Today: Proceedings*, vol. 5, pp. 24068–24074, 2018.

[4] H. Nu, M. Rinc, and G. Gonz, "Corrosion behavior of flame sprayed Cr_2O_3 coatings on carbon steel in chloride solutions," *Revista Ingenierías Universidad de Medellín*, vol. 21, pp. 143–162, 2022.

[5] G. Bolelli, D. Steduto, J. Kiilakoski, T. Varis, L. Lusvarghi, and P. Vuoristo, "Tribological properties of plasma sprayed Cr_2O_3, Cr_2O_3–TiO_2, Cr_2O_3–Al_2O_3 and Cr_2O_3–ZrO_2 coatings," *Wear*, vol. 480, pp. 1–18, 2021.

[6] S. I. Hango, L. A. Cornish, L. H. Chown, J. W. van der Merwe, and F. P. L. Kavishe, "Sliding wear resistance of the cobalt-based coatings, ULTIMET™ and STELLITE™ 6 with ruthenium additions," *Engineering Failure Analysis*, vol. 155, article 107717, 2024.

[7] P. M. Sousa, A. J. Silvestre, and O. Conde, "Cr_2O_3 thin films grown at room temperature by low pressure laser chemical vapour deposition," *Thin Solid Films*, vol. 519, no. 11, pp. 3653–3657, 2011.

[8] J. Lin and W. D. Sproul, "Structure and properties of Cr_2O_3 coatings deposited using DCMS, PDCMS, and DOMS," *Surface and Coating Technology*, vol. 276, pp. 70–76, 2015.

[9] D. Prabhakaran, N. Jegadeeswaran, B. Somasundaram, and B. S. Raju, "Corrosion resistance by HVOF coating on gas turbine materials of cobalt based superalloy," *Materials Today Proceedings*, vol. 20, pp. 173–176, 2020.

[10] S. Guo, D. Xu, G. Jiang, and W. Kuang, "Corrosion behavior and mechanism of Ni-based alloys Hastelloy C2000 and Inconel 740 in chloride-containing supercritical water oxidation," *Journal of Alloys and Compounds*, vol. 907, article 164452, 2022.

[11] Z. A. Abbasi, A. Mateen, A. Niaz, M. A. Ur Rehman, and A. Wadood, "Development and characterization of natural chromite coating on metal substrate using the plasma spray process," *ACS Omega*, vol. 8, no. 17, pp. 15193–15202, 2023.

[12] G. S. P. Kumar, A. Shinde, Y. Yadav, G. S. Hebbar, and M. H. Kumar, "Investigations on slurry erosive on wear performance of HVOF-sprayed Cr_2O_3 coatings on aluminum alloy," *Journal of Bio- and Tribo-Corrosion*, vol. 7, p. 106, 2021.

[13] Y. Wang, Y. Yang, H. Liang, W. Tian, and Y. Shao, "Effect of Cr_2O_3 on the microstructure and wear resistance of coatings prepared from Cr_2O_3–SiC–Al composite powders," *Materials Chemistry and Physics*, vol. 304, article 127860, 2023.

[14] H. Sun, G. Yi, S. Wan et al., "Effect of Cr_2O_3 addition on mechanical and tribological properties of atmospheric plasma-sprayed NiAl–Bi_2O_3 composite coatings," *Surface and Coatings Technology*, vol. 427, article 127818, 2021.

[15] P. Zamani and Z. Valefi, "Microstructure, phase composition and mechanical properties of plasma sprayed Al_2O_3, Cr_2O_3 and Cr_2O_3-Al_2O_3 composite coatings," *Surface and Coating Technology*, vol. 316, pp. 138–145, 2017.

[16] X. Wang, P. Ju, X. Lu, Y. Chen, and F. Wang, "Influence of Cr_2O_3 particles on corrosion, mechanical and thermal control properties of green PEO coatings on mg alloy," *Ceramics International*, vol. 48, no. 3, pp. 3615–3627, 2022.

[17] S. Dong, B. Song, B. Hansz, H. Liao, and C. Coddet, "Microstructure and properties of Cr_2O_3 coating deposited by plasma spraying and dry-ice blasting," *Surface and Coatings Technology*, vol. 225, pp. 58–65, 2013.

[18] I. P. Okokpujie, L. K. Tartibu, H. O. Musa-Basheer, and A. O. M. Adeoye, "Effect of coatings on mechanical, corrosion and tribological properties of industrial materials: a comprehensive review," *Journal of Bio-and Tribo-Corrosion*, vol. 10, no. 1, pp. 1–20, 2024.

[19] A. Amanov and S. P. Berkebile, "Improvement in tribological behavior of thermal spray Cr_2O_3 and Cr_3C_2–NiCr coatings by ultrasonic nanocrystal surface modification," *Materials Letters*, vol. 314, article 131919, 2022.

[20] M. S. Safavi and A. Rasooli, "The positive contribution of Cr_2O_3 reinforcing nanoparticles to enhanced corrosion and tribomechanical performance of Ni–Mo alloy layers electrodeposited from a citrate-sulfate bath," *Journal of Materials Research and Technology*, vol. 28, pp. 865–878, 2024.

[21] S. I. Hango, L. A. Cornish, J. W. van der Merwe, L. H. Chown, and F. P. L. Kavishe, "Corrosion behaviour of cobalt-based coatings with ruthenium additions in synthetic mine water," *Results in Materials*, vol. 21, article 100546, 2024.

[22] Z. Dong, W. Chen, W. Zheng, and D. Guzonas, "Corrosion behavior of chromium oxide based ceramics in supercritical water (SCW) environments," *Corrosion Science*, vol. 65, pp. 461–471, 2012.

[23] P. Zamani, Z. Valefi, and K. Jafarzadeh, "Comprehensive study on corrosion protection properties of Al_2O_3, Cr_2O_3 and Al_2O_3–Cr_2O_3 ceramic coatings deposited by plasma spraying on carbon steel," *Ceramics International*, vol. 48, no. 2, pp. 1574–1588, 2022.

[24] L. Mao, J. Xiao, G. Sun et al., "Microstructure and wear behaviors of Cr_2O_3–Al_2O_3 composite coatings deposited by atmospheric plasma spraying," *Surface and Coatings Technology*, vol. 444, article 128619, 2022.

[25] W. Su, S. Niu, Y. Huang et al., "Friction and wear properties of plasma-sprayed Cr_2O_3–$BaCrO_4$ coating at elevated temperatures," *Ceramics International*, vol. 48, no. 6, pp. 8696–8705, 2022.

[26] S. I. Hango, *Failure of Pump Systems Operating in Highly Corrosive Mine Water at Otjihase Mine*, University of the

Witwatersrand, Johannesburg, South Africa, 2018, http://wiredspace.wits.ac.za/handle/10539/25666.

[27] A. Suárez, A. Panfilo, E. Aldalur, F. Veiga, and P. Gomez, "Microstructure and mechanical properties of mild steel-stainless steel bimetallic structures built using wire arc additive manufacturing," *CIRP Journal of Manufacturing Science and Technology*, vol. 38, pp. 769–773, 2022.

[28] ASTM: G102-89, "Standard practice for calculation of corrosion rates and related information from electrochemical measurements," *ASTM*, vol. 89, pp. 1–7, 2015.

[29] J. Grubbs, K. Tsaknopoulos, C. Massar et al., "Comparison of laser diffraction and image analysis techniques for particle size-shape characterization in additive manufacturing applications," *Powder Technology*, vol. 391, pp. 20–33, 2021.

[30] C. Hegel, C. Jones, F. Cabrera, M. J. Yáñez, and V. Bucala, "Particle size characterization: comparison of laser diffraction (LD) and scanning electron microscopy (SEM)," *Acta Microscópica*, vol. 23, pp. 11–17, 2014, https://acta-microscopica.org/acta/article/view/208.

[31] X. Mei, X. Zhang, L. Zhang et al., "Enhancing the oxidation resistance of NiCrALY Bond coat by high-current pulsed electron beam irradiation," *Coatings*, vol. 11, no. 8, p. 912, 2021.

[32] F. Fanicchia, X. Maeder, J. Ast et al., "Residual stress and adhesion of thermal spray coatings: microscopic view by solidification and crystallisation analysis in the epitaxial CoNiCrAlY single splat," *Materials and Design*, vol. 153, pp. 36–46, 2018.

[33] P. S. Babu, D. Sen, A. Jyothirmayi, L. R. Krishna, and D. S. Rao, "Influence of microstructure on the wear and corrosion behavior of detonation sprayed Cr_2O_3–Al_2O_3 and plasma sprayed Cr_2O_3 coatings," *Ceramics International*, vol. 44, no. 2, pp. 2351–2357, 2018.

[34] O. J. Gerald, L. Wenge, Z. Yuan Tao, L. Cheng Long, and L. Qiang, "Influence of plasma spraying current on the microstructural characteristics and tribological behaviour of plasma sprayed Cr_2O_3 coating," *Boletín de la Sociedad Española de Cerámica y Vidrio*, vol. 60, no. 6, pp. 338–346, 2021.

[35] H. Zhang, J. Zhang, and Z. Wang, "Corrosion resistance of plasma-sprayed ceramic coatings doped with glass in different proportions," *Journal of Thermal Spray Technology*, vol. 32, no. 5, pp. 1286–1298, 2023.

[36] C. Monticelli, A. Balbo, and F. Zucchi, "Corrosion and tribocorrosion behaviour of thermally sprayed ceramic coatings on steel," *Surface and Coatings Technology*, vol. 205, no. 12, pp. 3683–3691, 2011.

[37] P. Zhang, S. X. Li, and Z. F. Zhang, "General relationship between strength and hardness," *Materials Science and Engineering A*, vol. 529, pp. 62–73, 2011.

[38] B. M. Setterfield-Price and R. A. W. Dryfe, "The influence of electrolyte identity upon the electro-reduction of CO_2," *Journal of Electroanalytical Chemistry*, vol. 730, pp. 48–58, 2014.

[39] D. Sri Maha, "Electrochemical synthesis of porous Ti-Nb alloys for biomedical applications," *Materials Science and Engineering: C*, vol. 96, pp. 466–478, 2019.

[40] W. Li, B. Brown, D. Young, and S. Nešić, "Investigation of pseudo-passivation of mild steel in CO_2 corrosion," *Corrosion*, vol. 70, no. 3, pp. 294–302, 2014.

[41] Q. H. Songa, F. S. Hao, Y. F. Zhang, Q. Lic, and J. J. Lia, "Electrochemical corrosion behavior of plasma sprayed Cr_2O_3–$25TiO_2$ composite coatings," *Digest Journal of Nanomaterials & Biostructures (DJNB)*, vol. 18, pp. 751–765, 2023.

[42] M. Grimm, S. Conze, L. Berger, G. Paczkowski, T. Lindner, and T. Lampke, "Microstructure and sliding wear resistance of plasma sprayed Al_2O_3–Cr_2O_3–TiO_2 ternary coatings from blends of single oxides," *Coatings*, vol. 10, no. 1, p. 42, 2020.